ZnCdSe-ZnSe Cladded Quantum Dots using Photoassisted Microwave Plasma (PMP) Enhanced Metalorganic Chemical Vapor Deposition for Lasers and Electroluminescent Phosphors

A. Rodriguez[1], R. Li[2], P. Yarlagadda[1], F. Papadimitrakopoulos[2], W. Huang[3], J. Ayers[1], and F. Jain[1]

[1]Electrical and Computer Engineering Department, University of Connecticut,
371 Fairfield Road, Storrs, CT, fcj@engr.uconn.edu
[2]Chemistry Department and Institute of Materials Science,
[3]US Military Academy, West Point, NY

ABSTRACT

We have grown for the first time 3-8 nm CdSe and pseudomorophic $Zn_xCd_{1-x}Se/Zn_yCd_{1-y}Se$ cladded quantum dots (CQDs) (x > y) in a novel Photo assisted Microwave Plasma Metalorganic Chemical Vapor Phase Deposition (PMP-MOCVD) reactor. Influence of growth parameters including microwave power, ultraviolet intensity, gas phase II/VI [Zn+Cd/Se] molar ratio, temperature of growth, and post-growth processing has been studied. High-resolution transmission electron microscopy (HR-TEM is used to compare the dots with colloidal dots reported in the literature. Simulation of the optical gain in an active layer hosting these dots is presented.

Keywords: ZnCdSe, cladded quantum dots, photo assisted microwave plasma MOCVD.

1. INTRODUCTION

Over the past years there has been a tremendous amount of work done on the fabrication, characterization and utilization of semiconducting quantum dots. Semiconducting Quantum-Dots (QD) provide quantum confinement in all three directions which results in the strongest possible enhancement of electrical and optical properties when compare to quantum well or quantum wire structures.[1] With quantum dots used in laser applications, the δ–like density of states function and the enhanced overlap of electron and hole wavefunctions has been shown to result in decreased threshold current densities, higher temperature stability of threshold current, as well as higher differential gain [1].

Further enhancement of the electrical and optical properties of QDs is achieved with the appropriate passivation of the QD surface [2]. Insufficient passivation leads to reduced quantum efficiency and thus poor overall performance of the QDs, mainly due to the recombination of the excitons due to surface states. In the fabrication of QDs by the Stranski-Krastanov growth mode the surfaces of QDs are inherently passivated by the growth of a wetting layer. Stranski-Krastanov growth does not permit lateral control of QD dimensions.

2. SIMULATION

In heteroepitaxial active and cladding layers a certain amount of strain exists in the layer depending on their lattice mismatch. The effect of dislocations is obviously detriment of the optical and transport properties of the device [3]. Huang *et al* [4] have shown that tensile strained active layers yield lower threshold current densities than active layers under compressive strain. Biaxial in-plane strain removes the degeneracy of the light hole and heavy hole bands which considerably influences the band gaps as well as band offsets. The variations in energy band gap and offsets at the heterointerfaces are important parameters in the gain calculation. Previous experiments have shown that the band offsets for II-VI heterointerfaces can be estimated from Harrison's theory [5]. Unlike the compressive strain, the light hole band is lifted above the heavy hole, resulting in a smaller band gap under tensile strain. In addition to the shifting of the energy band positions, the tensile strain also modifies the in-plane effective mass of the heavy hole, which becomes lighter, resulting in improved polarization factor ρ (see Eq.6) [4].

The strain in the layer is due to the lattice mismatch $(a_{film}-a_{sub})/a_{sub}$ which will produce a deformation of the film that will affect its optical and electrical properties. With the growth of zinc-blende heteroepitaxial structures of different lattice constants the in-plane lattice constant is assumed to be the same across the whole film. The strain in a given direction is given by the following equation:

$$\varepsilon_{ll} = \frac{a_{ll} - a_{sub}}{a_{sub}} \qquad (3.2)\{1\}$$

Here ε_{ll} is the in-plane strain and a_{ll} is the in-plane lattice constant of the film and a_{sub} is the lattice constant of the substrate, a similar expression of the perpendicular strain can be made. Even for lattice matched material systems it is probable that the film and the substrate will have different thermal expansion coefficients, which with a change in temperature will produce a strain in the film [3]. In the case of our quantum dot structures the differences in

the "substrate" (core) and the "film" (shell/cladding) are minimal, thus will not be taken into consideration.

The effect of strain on the band gap is calculated with the following equations shown to modify the band gap by either decreasing or increasing the band gap depending on the type of strain, compressive or tensile.

$$\Delta E_{LH} = \left[-2a\left(\frac{C_{11}-C_{12}}{C_{11}}\right) - 0.5b\left(\frac{C_{11}+2C_{12}}{C_{11}}\right)\right]\varepsilon_{ll} + \delta E_{SO} \quad (2)$$

$$\Delta E_{HH} = \left[-2a\left(\frac{C_{11}-C_{12}}{C_{11}}\right) + b\left(\frac{C_{11}+2C_{12}}{C_{11}}\right)\right]\varepsilon_{ll} \quad (3)$$

$$\delta E_{SO} = -\frac{\Delta_o}{2} + 0.5\sqrt{\left(\Delta_o^2 + \frac{9}{4}\left[2b\left(\frac{C_{11}+2C_{12}}{C_{11}}\right)\varepsilon_{ll}\right]^2 - 2b\left(\frac{C_{11}+2C_{12}}{C_{11}}\right)\varepsilon_{ll}\cdot\Delta_o\right)} \quad (4)$$

Here a and b are the hydrostatic and shear deformation potentials respectively, C_{11} and C_{12} are the elastic stiffness constants and Δ_o is the split orbital energy, ΔE_{LH} and ΔE_{HH} are the change in the light hole and heavy hole bands respectively [3]. Therefore in the simulations done, the strain in the cladding layer was calculated based on the lattice mismatch of the core. This is the main difference in these simulations compared with how the strain was used in previous simulations [6-9], where the strain is assumed to be in the core of the cladded quantum dot structure. It was assumed to be in the core because of how high quality dots were formed at the time of publication. Quantum dots were fabricated by selective growth techniques, such that pyramidal growth was used, and the quantum dot layer was grown on top of the pyramid structure followed by another layer of cladding growth. Thus the quantum dot was formed at the top of the pyramid. Therefore the strain in the system would be from the underlying pyramid material. A similar result is seen with the Stranski-Krastanov growth of self-assembled quantum dots, where the partial relaxation of strain energy compensates the increase in surface energy of the film, from which the quantum dot evolves. Thus there is less strain in the cladding of the quantum dot than in the core [10].

In our case the quantum dots are grown from a gas phase process, such that the core is grown first and then the cladding is deposited on the core. Therefore it is understandable that the core *serves* as the substrate and the cladding is analogous to the epitaxial film. Similar observations of this effect are seen in cladded quantum dots grown by colloidal chemistry methods [11]. Proof of this observation is seen in TEM images in which largely mismatch core/shell structures were fabricated and large amounts of dislocations were seen in the shell layer and not in the core.

The band gap related to quantum dot size developed by Brus is based on an effective mass model assuming the quantum dot is spherical is given as [6]:

$$E_{g(QD)} = E_{g(Bulk)} + \frac{\hbar^2\pi^2}{8R^2}\left[\frac{1}{m_e}+\frac{1}{m_h}\right] - \frac{1.8q^2}{4\pi\varepsilon_o\varepsilon R} \quad (5)$$

Here E_g is the energy bandgap of the quantum dot or bulk solid, R is the quantum dot radius, m_e is the effective mass of the electron in the solid, m_h is the effective mass of the hole in the solid, and ε is the dielectric constant of the solid. The second term on the right hand side of the equation provides the quantum energy of localization, which increasing for both the hole and electron as R^{-2}. The third term represents the Coulomb attraction.

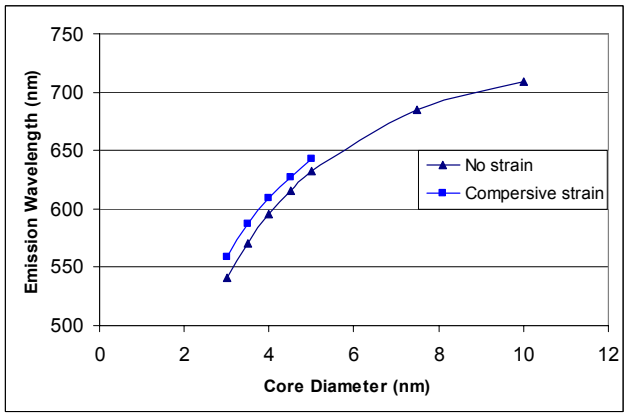

Figure 1: Comparison of emission wavelength with compressive strain in the core versus no strain in core of CdSe/ZnSe (core/shell) with varying core diameters.

Using equation 5 the energy band gap of CdSe/ZnSe (core/shell) system was calculated with CdSe cores of varying diameter, as shown in Figure 1. In the same figure the effects of compressive (based on the previous assumption of growth) strain in the core of the CdSe/ZnSe system was calculated for the same varying core diameter. It is plainly viewed that compressive strain has caused a red shift in the band gap of the system, which is consistent with the effects of compressive strain in quantum well structures. The effects of tensile strain on the core of a core/shell system is not shown, because that would mean that the core would be cladded by material that had an energy band gap less than the energy band gap of the core, which would then null the quantum confinement in the core.

In this work we have simulated the optical gain of cladded quantum dots including the modified effect of strain in the cladding for different compositions of cladding layers. The simulation is based on excitonic model (Equations 6 and 7) reported by Jain and Huang [6] with modifications to where the strain in the systems is accounted for as discussed earlier. The gain is obtained by taking the absorption coefficient term (α_{ex}) and multiplying it by the Fermi-Dirac distribution function, as shown in Equation 7.

$$\alpha_{ex}(\omega) = \frac{2\pi e^2}{\varepsilon_o n_r m_o c\omega}\sum_{l,h}\left\{\left(\frac{2}{(4\pi/3)a_{\mathbf{B},ex}^3}\right)|M_b|^2 \bullet \left|\int\psi_e(x)\psi_h(x)dx\right|^2 \bullet \left|\int\psi_e(y)\psi_h(y)dy\right|^2 \bullet \left|\int\psi_e(x)\psi_h(x)dx\right|^2 \rho_{ex} \bullet \frac{1}{\sqrt{\pi}\delta}e^{\left[(\hbar\omega_{ex}-\hbar\omega)^2/\delta^2\right]}\right\} \quad (6)$$

$$g = \alpha_{ex}(f_c + f_v - 1) \quad (7)$$

In Equation 6 $\delta = h/\tau\,(\ln 2)^{-1/2}$, τ is the intraband relaxation time (a value of 0.4 ps is used), $|M_b|^2$ is the average matrix element for the Bloch state, and ρ_{ex} is the exciton polarization factor under TE mode (whose value is 1/2 for electron-to-light hole and 3/2 for electron-to-heavy hole exciton transitions, respectively), as used in previous work of Huang *et al* [8] on quantum wire lasers. The density of states for excitonic transitions, expressed by the term shown in parenthesis before the M_b term in Equation 6, is derived by a similar treatment as used for the quantum wire case. The electron and hole wave functions are represented by $\Psi_e()$ and $\Psi_h()$ respectively.

In this simulation we assume the strain is in the shell of the CdSe/ZnSe system with a core diameter of 3.5 nm. The strain in the shell would imply the strain would be tensile in this case. Due to constraints of the strain equations above, we assume various Δ's in the conduction band and the valance band based on previous work.

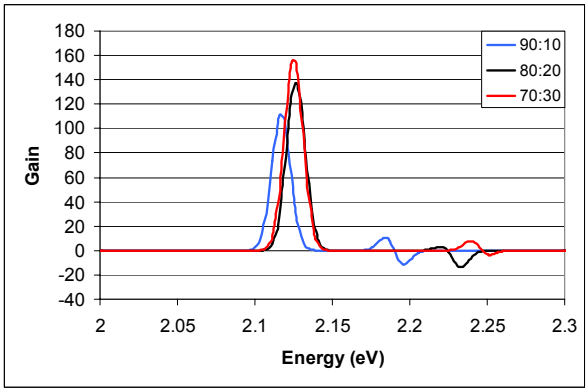

Figure 2: Comparison of tensile strain in the cladding using various ΔEc:ΔEv of CdSe/ZnSe (core/shell) with a CdSe diameter of 3.5nm.

Parameters	ZnSe	CdSe
a (eV)	-4.53	-3.664
b (eV)	-1.14	-0.80
C_{11} (10^{10} Pa)	8.52	6.67
C_{12} (10^{10} Pa)	5.17	4.63
m_e	0.17	0.11
m_{lh}	0.14	0.14
m_{hh}	0.45	0.75
Er	8.7	9.6
a_o A	5.668	6.05
Eg (eV)	2.72	1.692
X_i (eV)	4.09	4.95
Δ_{so} (eV)	0.42	0.42

Table 3.1 Parameters used in the calculations of strain and energy band diagrams of $Zn_xCd_{(1-x)}Se/Zn_yCd_{(1-y)}Se$ cladded quantum dots (x>y).

As the difference in the valance bands increases the gain of the system increases, this is due to improved confinement of the hole wave function as compared with the other cases. From these results it can be clearly understood that as the composition of the shell and the core material used are closer to the same composition the confinement of the hole function will continue to degrade. In previous work the compressive strain in the core of the system caused a red shift in the emitted wavelength, where tensile strain caused a blue shift in the emission [4,6-9]. With one of the benefits of utilizing quantum dots being that to decrease the wavelength of the emitted photons, the tensile strain effect was a welcomed phenomena. Now with the strain understood to exist in the cladding of the quantum dot system, the opposite is true, where tensile strain actually degrades the quality of the system.

3. EXPERIMENT

The QDs and CQDs are fabricated and deposited on n+-GaAs (100) substrates and carbon-backed TEM grids. The GaAs substrates were prepared for processing by cleaning sequentially in boiling TCE, acetone, and methanol. The samples were then chemically polished in a 5 H_2SO_4: 1 H_2O_2: 1 H_2O Caro's etch for three minutes at a temperature of 70°C. After rinsing the substrates in de-ionized (DI) water for a second time, the native oxide layer was removed by treatment in a 1HCl: 1H_2O etch for one minute. The substrates were then rinsed in DI water and stored in isopropanol until loading.

The PMP-MOCVD novel reactor developed utilized a microwave source at 2.45 GHz. The photo irradiation was achieved using an Oriel Hg arc lamp operated at 200W electrical power. The ultraviolet irradiation was brought into the reaction chamber using a fiber optic bundle. Neutral density filters were used to adjust the irradiation intensity. All irradiation intensities reported were measured using an intensity meter (manufactured by HTG) outside of the reaction chamber.

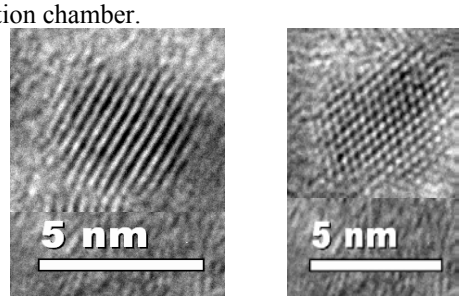

Figure 3: CdSe quantum dots grown using PMP-MOCVD technique.

A five-step technique was developed to fabricate the CQDs, which includes initial gas phase nucleation of core QDs with metal-organic (MO) precursors of dimethylzinc (DMZn), dimethyl-selenide (DMSe) and dimethylcadium (DMCd, and two sequential plasma sputtering and heat treatments without MO precursors (used for the cladding of the QDs). Influence of growth parameters including microwave power, ultraviolet intensity, gas phase II/VI

[Zn+Cd/Se] molar ratio, temperature of growth, and post-growth processing has been studied.

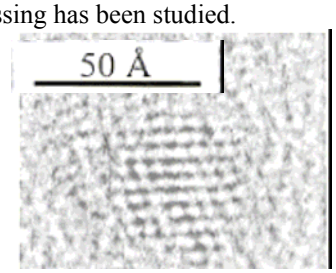

Figure 4: CdSe quantum dots grown by colloidal method [12].

The grown QDs are compared with those reported in the literature with colloidal chemistry methods (i.e. Figure 3. *vs* Figures 4) using high-resolution TEM. As can be seen we have obtained similar results. Photoluminescence (PL) peaks and Wide Angle X-ray diffraction (WAXRD) data have been used to calculate QD diameter and cladding thickness. Using Sherrer's formula the average overall diameter (D_{XRD})of the CQD can be estimated from the WAXRD using the following [13]:

$$D_{XRD} = \frac{0.9 * \lambda}{F * \cos(\theta_B)} \qquad (1)\{8\}$$

where λ is the x-ray wavelength, F is the FWHM of the XRD peak at 2-theta angle (θ_B). From the XRD peak position the composition of the QD is estimated using Vegard's law. This composition is then used to calculate the bulk energy band gap (E_{gB})of the QD. From the difference in the PL measured band gap and E_{gB} the core diameter is estimated with equation 5, described above.

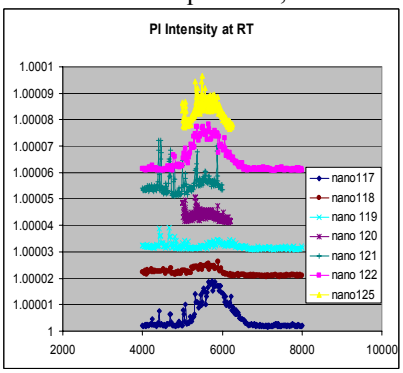

Figure 5: Photoluminescence intensity at 300K.

The influence on PL intensity of various growth conditions (represented by Samples # nano117-nano125) is shown in Figs. 5 (room temperature) and 6 (low temperature).

4. CONCLUSIONS

Pseudomorophic $Zn_xCd_{1-x}Se/Zn_yCd_{1-y}Se$ cladded quantum dots (CQDs) (x > y) have been grown using a novel Photo assisted Microwave Plasma Metalorganic Chemical Vapor Phase Deposition (PMP-MOCVD) reactor. High-resolution transmission electron microscopy (HR-TEM is used to compare the dots with colloidal dots reported in the literature. Influence of growth parameters including microwave power, ultraviolet intensity, gas phase II/VI [Zn+Cd/Se] molar ratio, temperature of growth, and post-growth processing has been studied. Optical gain in an active layer hosting these dots is computed using a modified excitonic model.

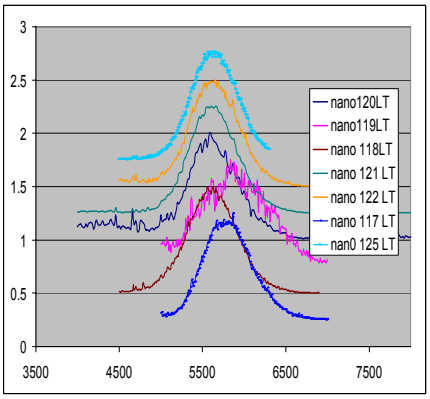

Figure 6: Photoluminescence intensity at 23K.

This work is supported in part by ONR Contracts N00014-05-1-0346 and N00014-06-1-0016, and NSF Grant EEC-0407279.

REFERENCES

[1] C. Burda, X. Chen, R. Narayanan, and M. El-Sayed. Chem. Rev., **105,** pp:1025-1102 (2005).
[2] G. W. Bryant. Journal of Luminescence. **70**, pp:108-119 (1996).
[3] M.C. Tamargo. II-VI Semiconductor Materials and Their Applications, Vol. 12, New York: Taylor & Francis (2002) Chapter 4.
[4] W. Huang and F.C. Jain. Guided-Wave Optoelectronics. (1995) pp: 125-132.
[5] W.A. Harrison. Electronic structure and the properties of solids. W.H. Freeman and company, San Francisco (1980).
[6] F. Jain and W. Huang Journal of Applied Physics. 85 (March 1999) pp: 2706-2712.
[7] W. Huang and F. Jain. Journal of Applied Physics. 87 (May 2000) pp: 7354-7359.
[8] W. Huang and F. Jain. Journal of Applied Physics. 81 (May 1997) pp: 6781-6785.
[9] W. Huang and F.C. Jain. Applied Physic Letters. 66 (March 1995) pp: 1596-1598.
[10] X.B. Zhang and S.K. Hark. Journal of Electronic Materials. 30 (10 November 2001) 1338-1342.
[11] I. Mekis, D. Talapin, A. Kornowski, M. Haase and H. Weller. Journal of Physical Chemistry B. 107 (2003) pp: 7454-7462.
[12] B.O. Dabbousi, J. Rodriguez-Viejo, F.V. Mikulec, J.R. Heine, H. Mattoussi, R. Ober, K.F. Jensen, M.G. Bawendi. J. Phys. Chem. B, **101**, 9463-9475.(1997).
[13] J. Friem, J. McKittrick, J. Katz and K. Sickafus, "Microwave sintering of nanocrystalline γ-Al_2O_3," Nanostructured Materials, **4**, pp:371-385, (1994).